Journal of Nondestructive Evaluation manuscript No.
(will be inserted by the editor)

Thermographic non-destructive evaluation of carbon fiber-reinforced polymer plates after tensile testing

Henrique Fernandes · Clemente Ibarra-Castanedo · Hai Zhang · Xavier Maldague

Received: date / Accepted: date

Abstract Infrared thermography (IT) is a safe non-destructive evaluation (NDE) technique that has a fast inspection rate and is generally contactless. It is used for diagnostics and monitoring in several fields including composite materials. In this paper carbon fiber-reinforced polymer (CFRP) plates submitted to tensile testing are inspected using IT. More specifically, carbon/PEEK (Polyether ether ketone) panels made of random-oriented strands (ROS) by compression moulding are submitted to tensile testing and then inspected using three different IT active approaches. The first two approaches use optical sources however with different scanning modes. The first active approach tested is a static surface scanning inspection in reflection mode. The second one is a dynamic line scanning technique where the energy source and camera are in movement with regards to the test sample. The last active IT approach tested uses a mechanical source (ultrasound excitation) to transfer heat to the sample being tested. This last approach is commonly called vibrothermography (VT). Results obtained were then compared to results obtained by micro computed tomography (μCT) inspection and microscopy. Results revealed voids associated with resin-rich regions as well as cracks.

Keywords Pulsed thermography · Line scan thermography · Vibrothermography · Composite materials · Tensile testing

H. Fernandes · Hai Zhang · C. Ibarra-Castanedo · X. Maldague
Computer Vision and Systems Laboratory (CVSL), Department of Electrical and Computer Engineering, Laval University; Quebec City (Quebec), G1K 7P4, Canada.
H. Fernandes ✉ E-mail: henrique-coelho.fernandes.1@ulaval.ca
Tel.: +1-418-6562131 ext 4786
C. Ibarra-Castanedo. E-mail: clemente.ibarra-castanedo@gel.ulaval.ca
H. Zhang. E-mail: hai.zhang.1@ulaval.ca
X. Maldague. E-mail: xavier.maldague@gel.ulaval.ca

1 Introduction

The use of composite materials, or composites, in the aeronautic industry has grown in the last years. Manufacturers have expanded the use of composites to the fuselage and wings because these materials are typically lighter and more resistant to corrosion than the metallic materials that have traditionally been used in airplanes. An example of the use of composites in commercial aircrafts is the Boeing 787 whose material mass percentage is more than 50% composed of composites (excluding the engines) [3]. This increasing demand motivates the industry to not only develop better and more cost efficient techniques to manufacture these materials but also to develop techniques to inspect and assure the quality of these materials during their entire life time. Cracks are one kind of defect that could appear in composite materials and may compromise their integrity. Thus one needs to detect these cracks in composites in order to assure the quality of the part.

Infrared thermography (IT) is a safe non-destructive evaluation (NDE) technique that has a fast inspection rate and is generally contactless. It is used for diagnostics and monitoring in several fields such as electrical components, thermal comfort, buildings, artworks, composite materials and others. IT's popularity has grown in the recent years due to spatial resolution and acquisition rate improvements of infrared cameras while they became more affordable. Another factor is the development of advanced image processing techniques focused on this kind of image. In active IT an external heat source is used to stimulate the material being inspected in order to generate a thermal contrast between the feature of interest and the background. The active approach is adopted in many cases given that the inspected parts are usually in equilibrium with the surroundings [8].

In this paper carbon fiber-reinforced polymer (CFRP) plates after tensile testing are inspected using IT. More specifically, carbon/PEEK (Polyether ether ketone) plates made of random-oriented strands (ROS) by compression moulding are submitted to tensile testing and then inspected using three different IT active approaches. Introduced in the late 2000s, ROS composites allows for manufacturing of high performance complex parts. ROS utilizes the performance benefits of continuous fibers while sharing the advantages of processability common to short discontinuous fibers. Conventional continuous fibers offer the mechanical performance but they are very difficult to form. On the other hand, parts with complex features can be injection moulded using lower volume content of short fibers, but they will lack mechanical properties. ROS composites lie in between these two material configurations.

The first two IT approaches used for inspection use optical sources however with different scanning modes. The first active approach tested is a static surface scanning inspection in reflection mode (the classical pulsed thermography configuration). The second one is a dynamic line scanning technique where the energy source and camera are in movement with regards to the test sample. The last active IT approach tested uses a mechanical source (ultrasound excitation) to generate heat in the sample being inspected. This last

approach is commonly called vibrothermography (VT). Results obtained with these three techniques were then compared to results obtained by micro computed tomography (μCT) inspection and microscopy. Results revealed voids associated with resin-rich regions as well as cracks.

The remainder of this paper is organized as follows: in the next section the IT techniques employed in this project are briefly discussed. In section 3 the inspected samples are described and experiments and results are presented in 4. Finally in section 5 conclusion and final remarks are provided.

2 Active thermography

In active thermography an external heat source is required to stimulate the material for inspection generating a thermal contrast between the feature of interest and the background. The active approach is adopted in many cases given that the inspected parts are usually in equilibrium with the surroundings [8]. In order to design a thermography experiment to achieve the best possible result some elements need to be considered. Figure 1 presents a diagram summarizing the different elements to take into account when designing a thermography inspection scenario. Since it is not the goal of this paper to make an extensive review on infrared thermography, just the three approaches used to inspect the specimens will be briefly described next.

2.1 Pulsed thermography (PT)

In pulsed thermography (PT) [1,4,7,16,17], the specimen surface is submitted to a heat pulse using a high power source such as photographic flashes. A heat pulse can be considered as the combination of several periodic waves at different frequencies and amplitudes. The pulse is absorbed by the specimen producing a fast surface temperature rise by photothermal heating, the thermal front then travels from the surface through the specimen by conduction. As time elapses, the surface temperature will decrease uniformly for a piece without internal flaws. On the contrary, subsurface discontinuities (e.g. porosity, delaminations, disbonds, fiber breakage, inclusions, etc.), can be seen as resistances to heat flow that produce abnormal temperature patterns at the surface, which can be detected with an IR camera.

Data acquisition in PT is fast and straightforward as illustrated in Figure 2. Flashes can be used to heat up the specimen's surface, and subsequently, the thermal changes are recorded with an infrared camera. Data is stored as a 3D matrix where x and y are the spatial coordinates, and t is the time. The cooling rate of a defective zone is different from a sound area.

2.2 Line scanning thermography (LST)

Line scan thermography (LST) [2,10,18,19] is a dynamic active thermography technique, which can be employed for the inspection of materials by heating a component, line-by-line, while acquiring a series of thermograms with an infrared camera. This can be done in two ways, either the thermographic head as described by Woolard and Cramer in [19], consisting of an infrared camera and an energy source, moves along the surface while the part is motionless or, as described by Oswald-Tranta and Shepard in [10], it may be the component that is in motion while the thermographic head stands still. In both cases, the thermal history for every pixel or line of pixels can be precisely tracked by controlling the heating source speed and the rate of data acquisition. In the original acquisition sequence the inspected sample appears to be moving so the sequence must be reconstructed in order to have the variation on time and not on space. The reconstructed matrix is obtained by following the temporal evolution of every pixel line independently, in such a way that, a given pixel line of the original sequence is recovered frame by frame (through time) and reallocated into a new sequence of images. Figure 3 shows a possible set-up for a LST inspection. In Figure 3 the thermographic head is composed by the a infrared camera and a heat source (an electrical actuator with a quartz infrared lamp of 1600W). The thermographich head moves in one sense (top to bottom) covering the entire surface of the sample to be inspected while the last remains motionless.

2.3 Vibrothermography (VT)

In contrast to the two first approaches where the energy is delivered to the sample externally, in vibrothermography the energy is generated internally. Vibrothermography (VT), also known as ultrasound thermography [15], utilizes mechanical waves to directly stimulate internal defects and without heating the surface as in optical methods. In VT, ultrasonic waves will travel freely through a homogeneous material, whereas an internal defect will produce a complex combination of absorption, scattering, beam spreading and dispersion of the waves, whose principal manifestation will be in the form of heat. Heat will then travel by conduction in all directions and an IR camera can be directed to one of the surfaces of the specimen to capture the defect signature. Ultrasonic waves are ideal for NDT since they are not audible to humans (although some low frequency harmonics are present), defect detection is independent from its orientation inside the specimen, and both internal and open surface defects can be detected. Hence, VT is very useful for the detection of cracks and delaminations. Figure 4 shows a schematic setup of a vibrothermography experiment where, similar to PT, an ultrasound wave burst is injected into the specimen (flash pulse in the PT case) and the temperature profiles are recorded with an infrared camera.

The ultrasound wave is produced by a transducer composed of a stack of piezo elements and concentrated in a titanium horn that acts like a hammer. Hence, the part being inspected should be firmly immobilized (but without damaging it) to avoid cantilever effects, clapping and sliding of the transducer. The transducer horn should be pressed against the sample as well to improve the coupling transmission of the ultrasound into the specimen. A bad coupling implies a poor ultrasound transmission but more seriously it creates unwanted heat in the vicinity of the ultrasound injection point.

After the elastic waves are injected to the specimen, they travel through the material and dissipate their energy mostly at the defects generating frictional rubbing, thus heat is locally released [9,13,12]. The thermal waves then travel by conduction to the surface where they can be detected with an IR camera.

When compared to optical/external techniques, the thermal wave travels half the distance in a VT experiment since heat propagation is performed from the defect to the surface, whereas for optical techniques heat travels from the surface to the defects and back to the surface. Thus, VT is very fast, even faster than PT. The duration of a typical experiment varies from a fraction of a second to several seconds. In addition, the longer the transducer operates at the surface, the more heat is released at the contact surface, increasing the probability of damaging the area. Furthermore, the pressure applied between the horn and the specimen has a great impact on the thermal response [15].

VT is extremely fast, although it is necessary to relocate the transducer (and to immobilize the specimen again) to cover a large area for inspection. Hence, VT is more suitable for relatively small objects. It is the most appropriate technique to inspect certain types of defects, e.g. micro cracks. On the contrary, it does not perform very well in some other cases in which application of optical techniques are straightforward, e.g. water detection. But probably the most inconvenient aspect of VT is the need to hold the specimen. On the other hand, there is only minimal heating of the inspected specimen since energy is usually dissipated mostly at the defective areas, although there is some localized heating at the coupling and clamping points.

3 Inspected panels

CFRP panels inspected in this paper were moulded using carbon/PEEK unidirectional slit tape from TenCate, which was cut into strands of desired lengths (6 or 50 mm) using an automated tape cutter. Strands were placed into the mould in small batches and shuffled each time to better control their distribution and to minimize their out-of-plane orientation. The mould was closed, placed into a pre-heated press and a pressure of 34 bars was applied. The mould temperature was increased up to 380°C and was maintained for 15 minutes. It was then cooled down at an approximate rate of 10°C/min and removed from the press. Figure 5 illustrates the manufacturing cycle.

Short strands panels (6 mm long strands) and longer strands panels (50 mm long strands) were moulded. Panels were then cut in 250 x 25 mm samples

for tensile testing , i.e. they were subjected to a controlled tension until failure. Crashed samples were then inspected using IT techniques in order to identify cracks that occurred after the failure. By visually examining the samples the region of failure was concentrated in one or two regions, however smaller cracks may have occurred in other regions of the panels and these smaller cracks are the focus of the IT inspections in this paper. Figure 6 shows ROS samples inspected in this paper. Figure 6a shows a short strand sound sample while Figure 6b shows a short strand sample after failure due to tensile testing. Figure 6c shows a long strand sample after failure due to tensile testing. Failures in Figure 6b and Figure 6c can be visually seen.

4 Results and discussion

Figure 7 shows the experimental set-ups used to inspect the parts. For all inspections a mid-wave infrared (MWIR) camera (FLIR Phoenix, InSb, 3-5 μm, 640 x 512 pixels) at a frame rate of 55 Hz was used to record the temperature profiles. In the pulsed thermography inspection case, two photographic flashes (Balcar FX 60 with pulse duration of 5 ms and producing 6.4 kJ per flash) were used to heat the sample. Images were recorded in reflection mode. In the second case, the line scan inspection, a thermographic head was used consisting of the same MWIR camera and an electrical actuator with a quartz infrared lamp (1600W). Samples were kept motionless while the thermographic head moved at a constant speed of 10 mm/s. In the vibrothermography case, the transducer horn was pressed against the sample and a burst of ultrasound waves (15 - 25 kHz, 2200 W) at a modulation frequency of 0.2 Hz and with amplitude modulated between 10-30% of maximum power was delivered to the sample for each inspection.

Samples from short and long strands were tested with the three active IT techniques (PT, LST and VT). First, results obtained from inspection of short strands panels are presented and then results obtained from inspection of long strand panels. Each infrared sequence was processed with principal component thermography (PCT) [11]. In this technique, the data sequence is decomposed into a set of orthogonal statistical modes (known as Empirical Orthogonal Functions or EOFs) obtained through Singular Value Decomposition (SVD). The most meaningful information is placed in the first EOF images.

Figure 8 shows the fourth EOF image obtained with PCT for a pulsed thermography inspection of two short strand samples. Figure 9 shows the fourth EOF image obtained with PCT for a line scan inspection of the same samples inspected in Figure 8 (both samples in Figure 9 were tested simultaneously). Figure 8a and 9a show results of an inspection of an untested sample while Figure 8b and 9b show results of a tested sample, i.e. after failure due to a tensile test previously performed.

Both pulsed thermography and line scan were able to reveal some of the strand/resin structure on the surface of the sample. However, it was not possible to detect micro cracks on the samples, only the large crack which is visible

to the naked eye. With pulsed thermography it was possible, however, to identify more resin-rich areas than when using line scan. On the other hand, line scan highlighted only some particular strands on the surface of the sample which are not related to cracks or resin-rich areas.

On the other hand, with vibrothermography inspection, it was possible to detect the small cracks spread throughout the sample. Figure 11 shows the unprocessed temperature images for the case of both untested sample (Figure 11a) and tested sample (Figure 11c). Also, temperature profiles of some pixels are presented to illustrate the difference between a resin-rich area (Figure 11b and Figure 11e) and a crack (Figure 11d). The regions corresponding to the temperature plots are marked on the images with small color arrows (it is possible to see the colors on the electronic version of the paper). While in a resin-rich spot the temperature increase was less than 1°C, in a small crack spot the temperature increase was almost 10°C. Figure 10 shows the result of the same inspections processed with PCT. Figure 10a shows PCT result image of untested sample and Figure 10b shows PCT result image a sample after tensile test. Since the large failure of the crashed sample (Figure 10b) separated the sample into two parts, only results from the larger part are presented (which corresponds to more than 80% of the sample size).

The results of inspections of long strand samples with pulsed thermography and line scan were similar to the ones achieved in the short strand samples case, i.e. only the large cracks were detected. Hence, they are not presented here. Figure 12 shows the results of a vibrothermography inspection of a long strand sample. An unprocessed temperature image is shown in Figure 12a and Figure 12b shows temperature profiles of a sound area and two cracks. Also, an EOF image obtained with PCT applied to the same inspection is shown in Figure 12c.

If one compares the vibrothermography results obtained from short and long strands some differences can be noticed. First, short strand samples presented more widespread damage after failure when compared with long strand samples. In the case of long strand samples, the region of failure was concentrated to one or two major cracks and no small cracks were detected in other regions of the sample. Also, very few resin-rich areas were detected. On the other hand, in the case of small strand samples, several small cracks were detected on the samples as well as the presence of several resin-rich areas. Second, it is possible to distinguish between large and small cracks and also resin-rich areas based on their temperature profiles. For large cracks, the temperature increase could be greater than 30°C (see Figure 12a and Figure 12b), for smaller cracks the temperature increase is around 10°C and for resin-rich areas the increase is less than 1°C.

Preliminary comparisons were performed with microscopy and μCT images. In both cases, the images support the results obtained with vibrothermography. While long strands samples show very few void/resin-rich areas, the short strand samples display a high percentage of voids/resin-rich area content. This could explain the fact that more small cracks were found in the short strand samples in the vibrothermography tests. Figure 13 shows exam-

ples of microscopy images and Figure 14 shows some μCT images both for long and short strands.

5 Conclusions

In this paper CFRP samples made of ROS carbon/PEEK were inspected with three different active IT techniques after failure due to tensile testing. PT and LST did not show a great potential for detection of small cracks while VT gave rise to very promising results. One factor that favors VT is the way heat is generated. While in the first two approaches heat is optically deposited on the surface of the sample, in VT the heat is generated internally due to frictional rubbing of the cracks which causes the heat to be concentrated around the defective areas. This suggests that the best IT technique for the detection of small cracks would be vibrothermography.

VT results suggest that in the case of panels moulded with long strands, i.e. 50 mm long strands, failure due to a tensile test is restricted to one or two regions. Also, small cracks were not detected in other regions of the sample and resin-rich areas are rarely present. On the other hand, in the case of panels moulded with short strands, i.e. 6 mm long strands, there is one main region where failure occurred but also several small cracks throughout the sample can be detected. Additionally, in short strands panel, resin-rich areas and voids are more present and they can be discriminated from small cracks based on their temperature profiles. Small cracks usually present a temperature increase around 10°C while resin-rich areas present temperature increase around 1°C.

Preliminary microscopy and μCT inspections were performed. Results confirm that a larger number of resin-rich areas and voids are present in short strands panels when compared to long strand panels. Which is coherent to results obtained with VT. Future work includes a quantitative comparison of the different IT techniques as well as a more detailed comparison with microscopy and μCT images.

Acknowledgements The authors would like to thank PhD student Marina Selezneva from the Structures and Composites Materials Laboratory of McGill University and NRC-Boucherville who manufactured the parts inspected in this work and performed microscopy and μCT inspections. The authors would like to gratefully acknowledge support provided by the Canada Research Chair in Multipolar Infrared Vision (MiViM) and the industrial partners: Bell Helicopter Textron Canada Limited, Bombardier Inc., Pratt and Whitney Canada Corp., Avior Integrated Products Inc., Delastek Inc. and Hutchinson Inc. Canada. The authors would also like to acknowledge the support of the following agencies: CNPq, National Council for Scientific and Technological Development - Brazil; NSERC, Natural Sciences and Engineering Research Council of Canada; FQRNT, Quebec Fund for Research on Nature and Technology and CRIAQ, Consortium for Research and Innovation in Aerospace in Quebec.

References

1. Balageas, D.L.: Defense and illustration of time-resolved pulsed thermography for nde. Quantitative InfraRed Thermography Journal **9**(1), 3–32 (2012). DOI 10.1080/17686733.2012.676902
2. Gruss, C., Balageas, D.: Theoretical and experimental applications of the flying spot camera. In: Proceedings of the QIRT 92, pp. 19–24 (1992)
3. Hale, J.: Boeing 787, from the ground up. Aero Magazine **24**(4), 16–23 (2006)
4. Ibarra-Castanedo, C., Bendada, A.H., Maldague, X.: Image and signal processing techniques in pulsed thermography. GESTS International Transactions on Computer Science and Engineering **22**(1), 89–100 (2005)
5. Ibarra-Castanedo, C., Maldague, X.: Infrared thermography. In: H. Czichos (ed.) Handbook of Technical Diagnostics, pp. 175–220. Springer Berlin Heidelberg (2013)
6. Ibarra-Castanedo, C., Tarpani, J.R., Maldague, X.: Nondestructive testing with thermography. European Journal of Physics **34**(6), S91 (2013). DOI 10.1088/0143-0807/34/6/S91
7. Lopez, F., Ibarra-Castanedo, C., Nicolau, V.P., Maldague, X.: Optimization of pulsed thermography inspection by partial least-squares regression. NDT & E International, **66**, 128 – 138 (2014)
8. Maldague, X.: Theory and practice of infrared technology for nondestructive testing, 1st edition edn. John Wiley & Sons, New York (2001)
9. Mian, A., Newaz, G., Han, X., Mahmood, T., Saha, C.: Response of sub-surface fatigue damage under sonic load a computational study. Composites Science and Technology **64**(9), 1115–1122 (2004)
10. Oswald-Tranta, B., Shepard, S.: Comparison of pulse phase and thermographic signal reconstruction processing methods. In: Proc. SPIE, Thermosense XXXV, vol. 8705, pp. 87,050S1–9 (2013)
11. Rajic, N.: Principal component thermography for flaw contrast enhancement and flaw depth characterisation in composite structures. Composite Structures **58**(4), 521–528 (2002)
12. Renshaw, J., Chen, J.C., Holland, S.D., Thompson, R.B.: The sources of heat generation in vibrothermography. NDT & E International **44**(8), 736–739 (2011)
13. Rothenfusser, M.J., Homma, C.: Acoustic thermography: vibrational modes of cracks and the mechanism of heat generation. In: AIP Conference Proceedings, vol. 760, pp. 624–631 (2005)
14. Selezneva, M., Kouwonou, K., Lessard, L., Hubert, P.: Mechanical properties of randomly oriented strands thermoplastic composites. In: S.V. Hoa, P. Hubert (eds.) Proc. 19th International Conference on Composite Materials (Montreal, Canada, July 2013), vol. 1, pp. 480–488 (2013)
15. Shepard, S., Ahmed, T., Lhota, J.R.: Experimental considerations in vibrothermography. In: Proc. SPIE, Thermosense XXVID, vol. 5405, pp. 332–335 (2004)
16. Shepard, S.M.: Advances in pulsed thermography. In: Proc. SPIE, Thermosense: Thermal Infrared Applications XXVIII, vol. 4360, pp. 511–515 (2001)
17. Vavilov, V.P., Burleigh, D.D.: Review of pulsed thermal NDT: Physical principles, theory and data processing. NDT & E International, **73**, 28 – 52 (2015)
18. Woolard, D.F., Cramer, K.E.: The thermal photocopier: A new concept for thermal ndt. In: Proc. SPIE, Thermosense XXVI, vol. 5405, pp. 366–373 (2004)
19. Woolard, D.F., Cramer, K.E.: Line scan versus flash thermography: Comparative study on reinforced carbon-carbon. In: Proc. SPIE, Thermosense XXVII, vol. 2782, pp. 315–323 (2005)

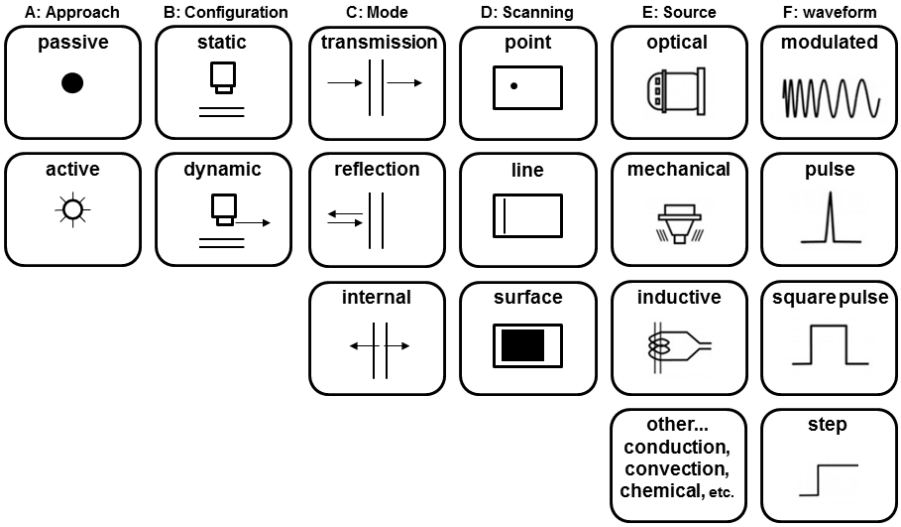

Fig. 1: Aspects to be addressed in the design of a infrared thermography experiment. Adapted from [6].

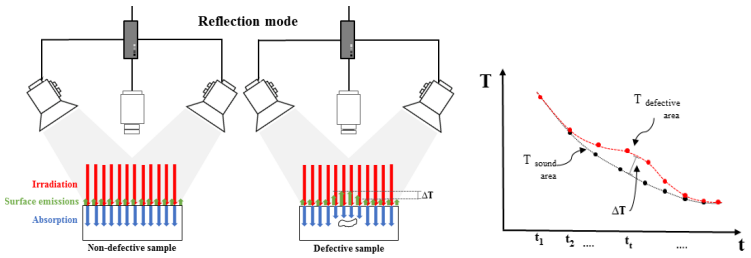

(a) (b)

Fig. 2: PT approach, in reflection mode, and temperature profiles of a sound and a defective area.

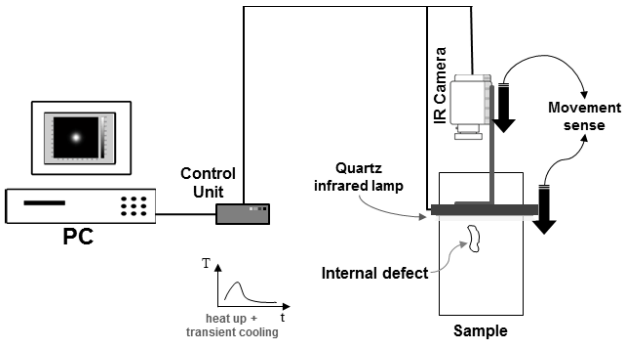

Fig. 3: Line Scan Thermography schematic set-up.

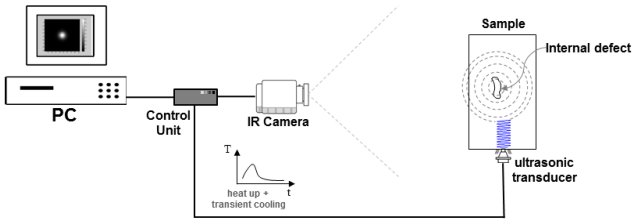

Fig. 4: Vibrothermography schematic set-up. Adapted from [5].

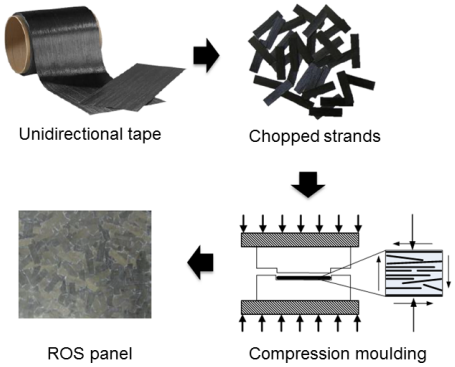

Fig. 5: ROS manufacturing cycle. Adapted from [14].

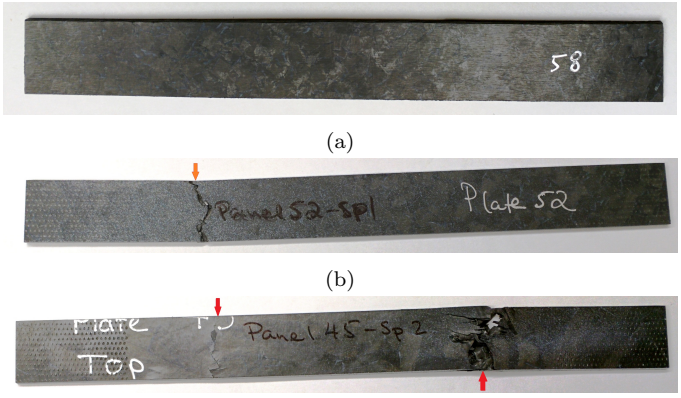

(a)

(b)

(c)

Fig. 6: ROS samples inspected. Arrows indicate the main region of failure. (a) Short strand sound sample, (b) short strand sample after failure due to tensile testing, and (c) long strand sample after failure due to tensile testing.

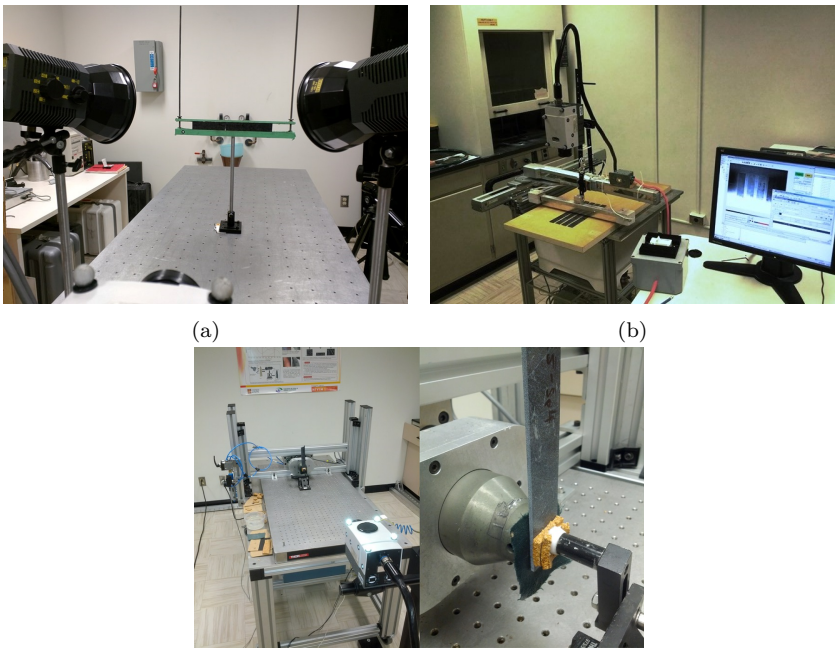

(a) (b)

(c)

Fig. 7: IT setups: (a) PT - Pulsed Thermography, (b) LST - Line Scan Thermography and (c) VT - Vibrothermography.

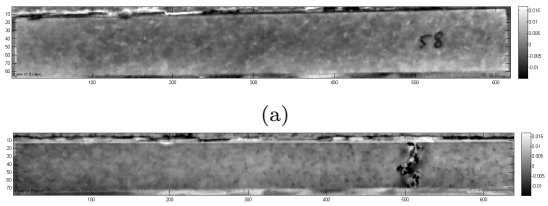

(a)

(b)

Fig. 8: Pulsed Thermography. PCT results (EOF 4) of short strands samples. (a) Untested sample and (b) after tensile test.

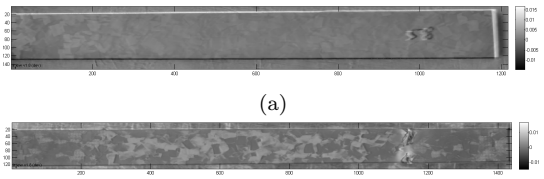

(a)

(b)

Fig. 9: Line Scan Thermography. PCT results (EOF 4) of short strands samples. (a) Untested sample and (b) after tensile test.

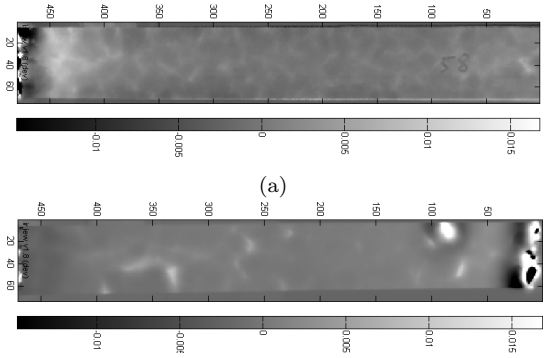

(a)

(b)

Fig. 10: Vibrothermography. PCT results (EOF 4) of short strands samples (same inspected in Figure 11. (a) Untested sample and (b) after tensile test.

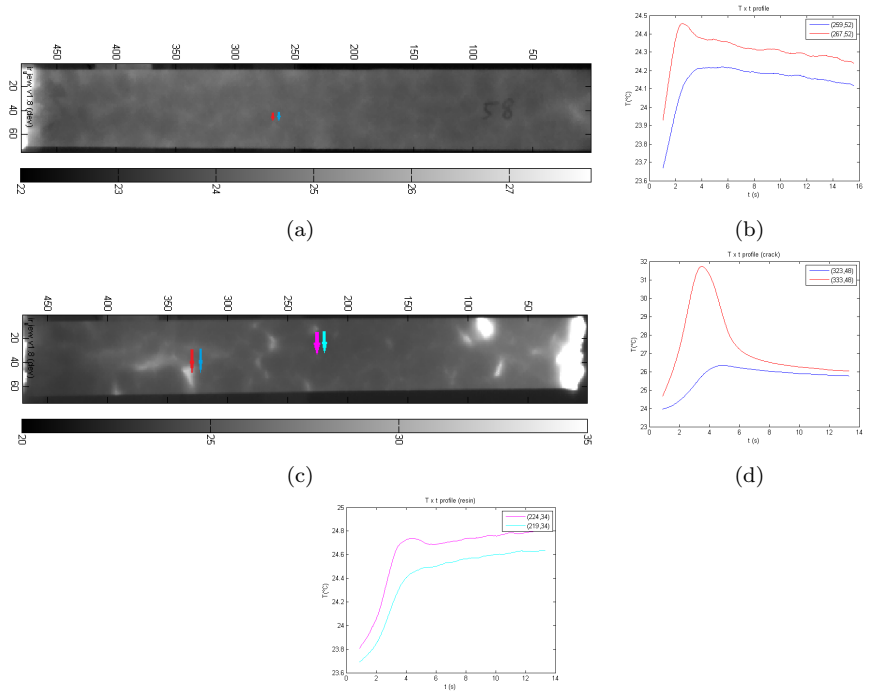

(a) (b) (c) (d) (e)

Fig. 11: Unprocessed temperature images of vibrothermography inspection of short strand samples. (a) Untested (sound) sample at 3.3 s, no cracks are detected, (b) temperature profiles of a resin-rich area and a sound area are present, (c) sample after tensile test at 2.6 s, (d): temperature profiles of a crack and a sound area are present, and (e) temperature profiles of a resin-rich area and a sound area are present.

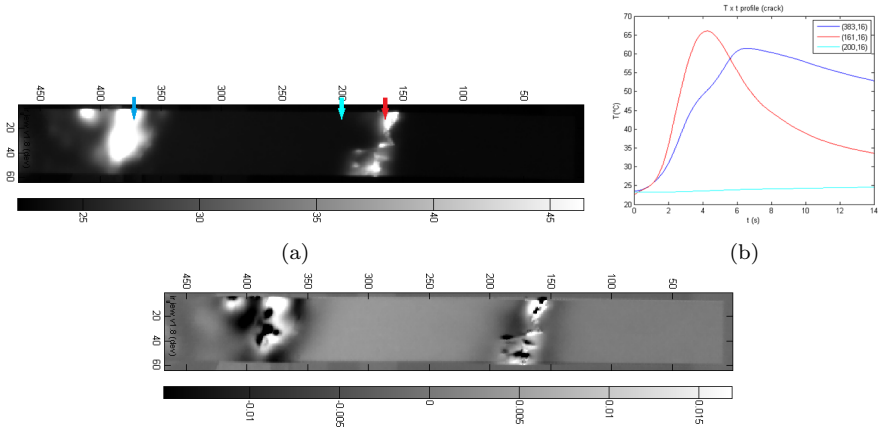

(a) (b)

(c)

Fig. 12: Vibrothermography results of long strand samples. (a) Unprocessed temperature image, (b) temperature plot of three points: (383,16) crack #1 which was closer to ultrasound horn coupling region, (200,16) a sound area and (161,16) crack #2 which was the region of main failure in the tensile test, and (c) PCT result (EOF 4) of the same sample.

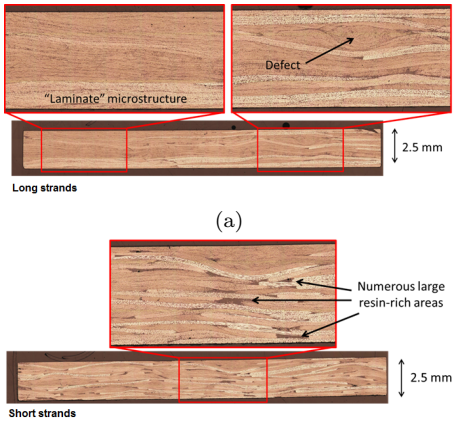

(a)

(b)

Fig. 13: Microscopy images. (a) Long strand samples display very few voids and resin-rich-areas while (b) short strand samples display a much higher content of resin-rich areas.

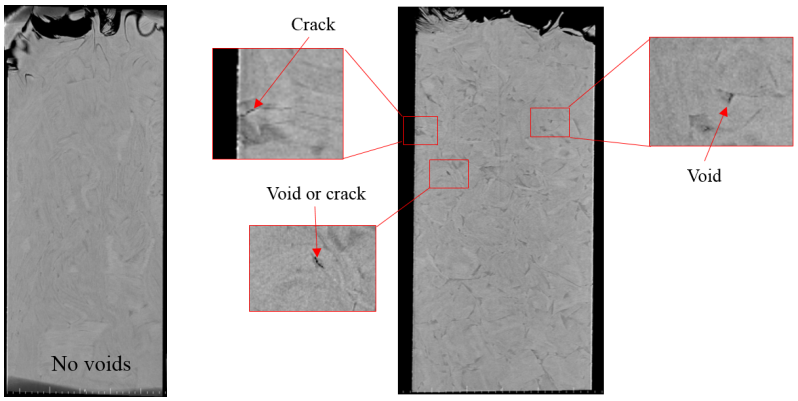

(a) (b)

Fig. 14: μCT images. (a) Long strands and (b) short strands. The second presents a higher content of voids and resin-rich areas.